



**HAL**  
open science

# In Silico Drug Repurposing for SARS-CoV-2 Main Proteinase and Spike Proteins

Irene Maffucci, Alessandro Contini

► **To cite this version:**

Irene Maffucci, Alessandro Contini. In Silico Drug Repurposing for SARS-CoV-2 Main Proteinase and Spike Proteins. *Journal of Proteome Research*, 2020, 19 (11), pp.4637-4648. 10.1021/acs.jproteome.0c00383 . hal-02933669

**HAL Id: hal-02933669**

**<https://hal.science/hal-02933669>**

Submitted on 30 Sep 2021

**HAL** is a multi-disciplinary open access archive for the deposit and dissemination of scientific research documents, whether they are published or not. The documents may come from teaching and research institutions in France or abroad, or from public or private research centers.

L'archive ouverte pluridisciplinaire **HAL**, est destinée au dépôt et à la diffusion de documents scientifiques de niveau recherche, publiés ou non, émanant des établissements d'enseignement et de recherche français ou étrangers, des laboratoires publics ou privés.

# In Silico Drug Repurposing for SARS-CoV-2 Main Proteinase and Spike Proteins

Irene Maffucci\* and Alessandro Contini\*

Cite This: <https://dx.doi.org/10.1021/acs.jproteome.0c00383>

Read Online

ACCESS |



Metrics &amp; More



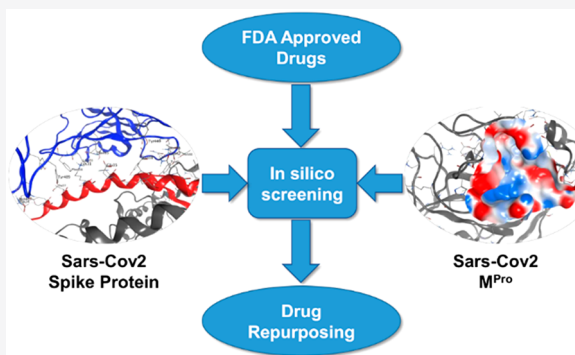
Article Recommendations



Supporting Information

**ABSTRACT:** The pandemic caused by SARS-CoV-2 is currently representing a major health and economic threat to humanity. So far, no specific treatment to this viral infection has been developed and the emergency still requires an efficient intervention. In this work, we used virtual screening to facilitate drug repurposing against SARS-CoV-2, targeting viral main proteinase and spike protein with 3000 existing drugs. We used a protocol based on a docking step followed by a short molecular dynamic simulation and rescoring by the Nwat-MMGBSA approach. Our results provide suggestions for prioritizing *in vitro* and/or *in vivo* tests of already available compounds.

**KEYWORDS:** SARS-CoV-2, COVID-19, virtual screening, main proteinase, 3CL<sup>pro</sup>, spike protein, molecular dynamics, MM-GBSA, drug repurposing



## INTRODUCTION

The outbreak of a novel  $\beta$ -coronavirus, SARS-CoV-2, is currently a pandemic threat, with already more than 23 million confirmed cases and more than 800 000 deaths all over the world, according to the World Health Organization (data of August 2020, <https://covid19.who.int>). Unfortunately, although many clinical and preclinical studies are ongoing, to date there is not a validated treatment to this infection.

As for other known coronaviruses, such as SARS-CoV and MERS-CoV, the SARS-CoV-2 entry into host cells is mediated by its transmembrane spike glycoprotein (S-protein). This is a trimeric protein belonging to the class I fusion proteins, whose structure for SARS-CoV-2 has been partially resolved by cryo-electron microscopy (code PDB 6VXX and 6VSB).<sup>1,2</sup> The S-protein is divided into two functional subunits: the S<sub>1</sub> subunit, which contains the receptor binding domain (RBD) responsible for the interaction with host cell's receptors, and the S<sub>2</sub> subunit, which is implicated in the fusion of the viral and cellular membranes.

Recent works showed that SARS-CoV-2 S-protein is able to bind the human angiotensin-converting enzyme 2 (hACE2),<sup>3–5</sup> explaining the symptoms linked to the SARS-CoV-2 infection (COVID-19), since hACE2 is widely expressed in endothelial cells from small and large arteries, in lung alveolar epithelial cells, but also in the heart, kidney, testis, and gastrointestinal system.<sup>6,7</sup> Moreover, the crystallographic structure of the RBD in complex with the hACE2 has been recently resolved (PDB code 6MOJ),<sup>4</sup> giving molecular details about this interaction (Figure 2). The binding to the host cell receptor triggers a series

of conformational changes which allow the fusion with the host cell and the entry of the virus.<sup>1</sup>

In addition, a recognized target for coronaviruses treatments is the main proteinase M<sup>Pro</sup>, also known as 3CL<sup>Pro</sup>.<sup>8,9</sup> This protein processes the polyprotein 1ab into mature nonstructural proteins that are essential for viral replication<sup>10</sup> and is rather conserved among coronaviruses. Moreover, human proteases with the same specificity have not been discovered so far, making M<sup>Pro</sup> an ideal target to treat coronavirus infections. The crystal structure of the SARS-CoV-2 M<sup>Pro</sup> in complex with a covalent peptidomimetic inhibitor (PDB code 6LU7<sup>11</sup>) was made available. Additionally, the Zhang group, developer of the popular homology-modeling software I-TASSER,<sup>12</sup> made available 24 3D structural models<sup>13</sup> of proteins in the SARS-CoV-2 genome.<sup>14</sup> Among these, the model of the M<sup>Pro</sup> (code QHD43415) was made available before the release of the crystal and was characterized by a very high reliability score (TM-score = 0.96).

It is clear that both spike and M<sup>Pro</sup> proteins represent potential targets for anti-SARS-CoV-2 drugs: on one side, hampering the interaction between hACE2 and the viral RBD will block the entry of the virus into the human cells. On the other side,

**Special Issue:** Proteomics in Pandemic Disease

**Received:** June 1, 2020

**Published:** September 7, 2020

67 inhibiting the viral proteases, as done with many antiviral drugs  
68 currently used in the therapy of HIV infection,<sup>15</sup> will interfere  
69 with the viral replication.

70 However, the experimental procedure to conceive a new drug  
71 is long (up to decades) and expensive (up to several millions of  
72 dollars). Such a time and resources price is not affordable in the  
73 current emergency situation; therefore, a promising alternative  
74 consists in a drug repurposing investigation exploiting *in silico*  
75 techniques, such as Virtual Screening (VS), which already  
76 proved to be able to identify active molecules against a  
77 target.<sup>16,17</sup>

78 Within this context and aiming to give our contribution to the  
79 current sanitary crisis, we designed a VS campaign of currently  
80 worldwide approved drugs. Despite the fact that similar studies  
81 have been recently published,<sup>18,19</sup> in this work we independently  
82 screened more than 3000 molecules against the two SARS-CoV-  
83 2 proteins mentioned above to provide information useful for a  
84 multiple treatment approach. In addition, we applied a solid VS  
85 procedure we recently developed and which was shown to be  
86 successful in discriminating active from inactive compounds  
87 within the screening of classical small molecules and protein–  
88 protein interaction inhibitors.<sup>20</sup>

## 89 ■ METHODS

### 90 Receptor Preparation

91 Receptor models for the SARS-CoV-2 M<sup>pro</sup> were prepared  
92 starting from both the 6LU7 crystal structure and the  
93 QHD43415 I-Tasser model. This choice was made to take  
94 binding site flexibility into account through an ensemble  
95 docking approach<sup>21</sup> but without the need to perform time-  
96 consuming molecular dynamic (MD) simulations to generate  
97 reliable conformational ensembles. The two M<sup>pro</sup> models were  
98 prepared using the MOE2019 software,<sup>22</sup> with the following  
99 protocol:

100 6LU7: all water molecules were deleted. The covalently  
101 bound peptidomimetic ligand was then unbound from Cys145,  
102 and the  $\alpha,\beta$  double bond of the ligand, that behaves as a Michael  
103 acceptor, was restored. The Structure Preparation module of  
104 MOE was used to correct PDB inconsistencies and to assign the  
105 protonation state at pH = 7.0. The default Amber10EHT force  
106 field, coupled to the Born solvation model was assigned to the  
107 system. The ligand was then minimized, keeping the receptor  
108 constrained. Then, the receptor was minimized by applying  
109 backbone restraints and keeping the ligand constrained. Finally,  
110 the complex was minimized in two separate steps, first by  
111 keeping backbone restraints, second by removing all restraints.  
112 All minimizations were performed up to a gradient of 0.1 kcal  
113 mol<sup>-1</sup> Å<sup>-2</sup>. The receptor and the ligand were then saved for  
114 future use.

115 4MDS: the crystal structure of SARS-CoV 3CL<sup>pro</sup> protei-  
116 nase,<sup>23</sup> a close homologue of SARS-CoV-2 M<sup>pro</sup>, in complex with  
117 a carboxamide inhibitor was also modeled to be used as an  
118 additional reference; this was done because no specific SARS-  
119 Cov2M<sup>pro</sup> noncovalent inhibitors were published at the time of  
120 this screening.<sup>24</sup> The system was prepared for calculations as  
121 follow: the PDB was corrected and protonated at pH = 7.0 using  
122 MOE as stated above. The ligand was minimized, keeping the  
123 receptor constrained, using the MMFF94x force field coupled  
124 with the Born solvation model. The receptor was then  
125 minimized, keeping the ligand constrained, using Amber10-  
126 EHT+Born. Finally, the complex was minimized in two steps, as  
127 described above.

QHD43415: the I-TASSER model QHD43415\_5<sup>13</sup> was  
128 superposed to 4MDS (prepared as previously described) in  
129 order to precisely define the binding site. Since we observed that  
130 the 4MDS ligand also fitted QHD43415\_5, the ligand was  
131 transferred, and the complex was prepared as described for  
132 4MDS. The resulting structure was used for docking.  
133

The RBD of the S-protein was obtained by the recently  
134 resolved X-ray structure of the complex between the SARS-  
135 CoV-2 RBD and the human ACE2 (code PDB 6M0J).<sup>4</sup> After the  
136 deletion of this latter, the RBD has been protonated at  
137 physiological conditions using the H++ server.<sup>25</sup>  
138

### RBD binding site definition 139

In order to determine the RBD residues playing the most  
140 important role in the binding to ACE2 (hot spots), the complex  
141 between RBD and ACE2 has been initially protonated as the  
142 single RBD. Successively, it has been submitted to a molecular  
143 dynamics (MD) simulation using the AMBER18<sup>26</sup> package and  
144 the ff14SB<sup>27</sup> force field. The system has been neutralized by  
145 adding the proper number of Na<sup>+</sup> ions and solvated adding a  
146 cubic box of TIP3P water up to a distance of 10 Å from the  
147 solute. The system has been relaxed by optimizing the geometry  
148 of hydrogens, ions, and water molecules (1000 cycles of steepest  
149 descent and 4000 cycles of conjugated gradient). The solvent  
150 box has been equilibrated at 300 K by 100 ps of NVT (constant  
151 volume and temperature) and 100 ps of NPT (constant pressure  
152 and temperature) simulation. Then, a minimization of side  
153 chains, water, and ions (2500 cycles of steepest descent and  
154 2500 cycles of conjugated gradient) and a global minimization  
155 (2500 cycles of steepest descent and 2500 cycles of conjugated  
156 gradient) were performed with a restraint of 10 kcal/mol applied  
157 on the backbone atoms. Successively the system has been heated  
158 up to 300 K in 6 steps of 20 ps each ( $\Delta T = 50$  K) during which  
159 the backbone restraints were reduced progressively from 10 to 5  
160 kcal/mol. The systems were then equilibrated for 100 ps in the  
161 NVT ensemble and for 200 ps in the NPT ensemble keeping a 5  
162 kcal/mol restraint on the backbone atoms. This was followed by  
163 a 4 steps NPT equilibration during which the restraints were  
164 progressively reduced to 1 kcal/mol. Finally, after a 500 ps  
165 unrestrained NPT equilibration, a production run of 20 ns was  
166 performed. During the whole simulation, an electrostatic cutoff  
167 of 8 Å, a time step of 2 fs, and the SHAKE algorithm were  
168 applied.<sup>28</sup> The root mean squared deviation (RMSD) of the  
169 backbone atoms using the X-ray structure as reference was used  
170 as a metric of simulation convergence (Figure S1). Hydrogen  
171 bonds (H-bond) analysis was performed on the last 10 ns of the  
172 simulation using the cpptraj module of AmberTools and using a  
173 donor–acceptor distance cutoff of 3.5 Å and a donor–donor  
174 hydrogen-acceptor angle cutoff of 150 deg (Table S2).  
175

After having defined as interfacial those RBD residues whose  
176 difference in the solvent accessible area when going from the  
177 complex to the isolated state was greater than 0.75 Å, an *in silico*  
178 alanine scanning was performed on the last 10 ns of the  
179 production run. The mutated complexes have been built using  
180 PyMol,<sup>29</sup> and the alanine scanning was run with the Amber  
181 mmpbsa.py code on one frame every 100 ps and by choosing the  
182 GB-Neck2<sup>30</sup> as implicit solvent model (igb = 8), the mbondi2 as  
183 radii set, and a salt concentration of 0.15 M. The  $\Delta\Delta G$  was  
184 calculated as the difference between the  $\Delta G$  of the mutated  
185 system and the one of the native system (Table S1). The  
186 residues giving  $\Delta\Delta G$  greater than 2.5 kcal/mol were considered  
187 as hot spots and were used to define the RBD potential binding  
188 site for small molecules.  
189

## 190 Database Preparation

191 Two separate databases were downloaded from the correspond-  
192 ing sources<sup>31,32</sup> and merged. The database was then checked and  
193 redundant molecules, identified by CAS number, were removed.  
194 The database was then processed by MOE in order to build the  
195 3D structures and to minimize the geometry of each molecule.  
196 The *wash* function of the MOE database tool was used with the  
197 MMFF94x+Born force field, requesting the dominant protona-  
198 tion state at pH = 7.0 and preserving existing chirality. The  
199 final database, consisting of 3118 unique molecules, was saved in  
200 SDF format.

## 201 Virtual Screening

202 The Virtual Screening (VS) was done according to our recently  
203 developed protocol.<sup>20</sup> This is applied using a set of scripts  
204 (available for download as [Supporting Information](#) within ref  
205 20) that does the following steps automatically: (1) Preparation  
206 of the screening library, including the generation of tautomers,  
207 alternative protonation states, stereoisomers and ring con-  
208 formers, if requested. (2) Docking of all molecules using  
209 PLANTS.<sup>33</sup> (3) Analysis of results. (4) Parameterization of  
210 docked ligands selected for rescoring. (5) Molecular dynamics  
211 of complexes selected for rescoring, using Amber.<sup>26</sup> Rescoring  
212 using the Nwat-MMGBSA method.<sup>20,34,35</sup> All dockings were  
213 performed by PLANTS, requesting a search speed = 1  
214 (maximum accuracy) and the ChemPLP scoring function.<sup>36</sup>  
215 Only the principal tautomer and protonation state predicted at  
216 pH = 7 were considered for the docking. The following receptor-  
217 specific parameters were also set up: 6LU7: binding site center  
218 (b.s.c.; x,y,z) = -10.2858, 12.3088, 69.3271; binding site radius  
219 (b.s.r.; Å) = 16. QHD43415: b.s.c. = -15.124, 15.0521,  
220 -24.6152; b.s.r. = 14. RBD-BS1: b.s.c. = -38.621, 39.731,  
221 1.564; b.s.r. = 17. RBD-BS2: b.s.c. = -36.355, 20.471, 2.322;  
222 b.s.r. = 17.

223 Nwat-MMGBSA rescoring was requested for the top 2% of  
224 compounds (about 60 molecules for each target). Rescoring  
225 consists in performing a short MD simulation (about 2.5 ns,  
226 including 1.5 ns of equilibration and 1 ns of production),  
227 followed by calculation of binding energy by MMGBSA.<sup>37</sup> In a  
228 previous work we demonstrated that longer MD simulations are  
229 not necessary for this purpose.<sup>20</sup> Nwat-MMGBSA binding  
230 energies were computed by including no explicit waters (Nwat =  
231 0, corresponding to standard MMGBSA calculations) or by  
232 selecting a certain number of explicit waters to be included in the  
233 calculation (Nwat = 10, 20, 30, 60, and 100).

234 The same protocol was applied to 4MDS also, since the  
235 binding energy computed for the 4MDS crystallographic ligand  
236 was used as a reference. Analogously, the binding energy of the  
237 6LU7 ligand (whose covalent bond was broken as described  
238 above), was computed as a reference.

## 239 ■ RESULTS AND DISCUSSION

### 240 Virtual Screening on M<sup>Pro</sup>

241 The VS campaign on SARS-CoV-2 M<sup>Pro</sup> was conducted on two  
242 different models (e.g., 6LU7 and QHD43415) to take binding  
243 site flexibility into account through an ensemble docking  
244 approach, increasing the solidity of the procedure with respect  
245 to previous VSs on the same protein.

246 The results of the VS campaign are summarized in [Table 1](#) and  
247 [Table 2](#), respectively, while [Tables S2 and S3](#), Supporting  
248 Information, report compounds selected by docking but that  
249 failed during the MD/Nwat-MMGBSA rescoring step. Results

**Table 1. Results of the VS Campaign on the Crystal Structure of SARS-CoV-2 M<sup>Pro</sup> (6LU7)<sup>a</sup>**

Drug Name	Dock score	Nwat-MMGBSA <sup>b</sup>
<b>Angiotensin II</b>	<b>-124.4</b>	<b>-120.3 ± 10.1</b>
<b>GHRP-2</b>	<b>-132.6</b>	<b>-106.0 ± 8.3</b>
<b>Indinavir</b>	<b>-122.4</b>	<b>-86.5 ± 5.7</b>
<b>Polymyxin B</b>	<b>-107.9</b>	<b>-84.2 ± 8.3</b>
<b>Fexofenadine</b>	<b>-107.8</b>	<b>-77.0 ± 7.8</b>
<b>Atazanavir</b>	<b>-109.6</b>	<b>-73.0 ± 7.6</b>
<b>Cobicistat</b>	<b>-124.3</b>	<b>-72.8 ± 8.3</b>
<b>Aliskiren</b>	<b>-109.9</b>	<b>-70.9 ± 6.5</b>
Lercanidipine	-106.6	-67.4 ± 8.4
Darunavir	-108.1	-66.6 ± 6.8
Montelukast	-112.8	-54.9 ± 6.8
Latanoprost	-108.5	-52.5 ± 4.2
Octenidine	-114.0	-50.8 ± 4.9
Velpatasvir	-108.4	-46.5 ± 8.1
Tyloxapol	-112.3	-42.5 ± 6.5
Salvianolic acid B	-124.4	-41.1 ± 11.0
Nilotinib	-106.6	-40.1 ± 8.6
Siponimod	-105.9	-38.5 ± 6.0
Travoprost	-114.9	-35.6 ± 6.1
Vitamin A Palmitate	-107.6	-35.5 ± 6.1
Penfluridol	-110.1	-30.2 ± 7.3
Clindamycin	-106.2	-20.5 ± 15.4
Ledipasvir	-109.6	-20.1 ± 7.8
Elbasvir	-106.3	-19.8 ± 9.9

<sup>a</sup>Top 2% of compounds selected from the docking of 3118 FDA approved drugs and rescored by Nwat-MMGBSA (Nwat = 30) are shown. Compounds that ranked better than the reference are highlighted in bold. The 6LU7 crystallographic ligand of the SARS-CoV-2 main protease (6LU7) was used as the reference. Docking and Nwat-MMGBSA scores are -132.7 and -70.6 ± 8.0 kcal/mol, respectively. <sup>b</sup>Nwat-MMGBSA rescoring was done considering 30 explicit water molecules around the ligand (Nwat = 30).

of Nwat-MMGBSA rescoring, using 30 explicit waters, are the  
250 only reported, since Nwat = 30 was considered a reasonable  
251 value in previous publications.<sup>20,34</sup> 252

253 As can be observed, the protease inhibitors indinavir and  
254 atazanavir, currently used to treat HIV infections, have been  
255 selected by both models. Conversely, the protease inhibitor  
256 lopinavir is top ranked for the QHD43415 model only, while it  
257 failed during MD for 6LU7 ([Table S2](#), SI), probably due to steric  
258 clashes originating from a position of the side chains in the  
259 crystal structure not favorable for a stable binding of this  
260 compound. [Figure 1](#) shows the predicted binding mode for  
261 lopinavir, that anchors to the M<sup>Pro</sup> binding site by multiple H-  
262 bonds. The first H-bond is observed between the catalytic His41  
263 residue and the aryloxyacetyl amido carbonyl (H-bond length =  
264 2.1 Å). Additional H-bonds are observed with Glu166 and the  
265 hydroxyl group at C-4, that acts both as a donor and an acceptor  
266 (lop-O(H)⋯(H)N-Glu166 and lop-OH⋯O=C-Glu166 dis-  
267 tances = 1.8 Å and 2.2, respectively). Finally, a dual H-bond is  
268 observed between the side chain of Gln189 and both the  
269 butanamido NH (lop-NH⋯O=C-Gln189 = 1.9 Å) and the 2-  
270 oxo-1,3-diazinanyl carbonyl (lop-C=O⋯H<sub>2</sub>N-Gln189 = 2.0  
271 Å).

272 In addition, within an *in vitro* study against SARS-CoV-2, it  
273 has been shown that lopinavir has an estimated 50% effective  
274 concentration (EC<sub>50</sub>) of 26.63 μM in Vero E6 cells.<sup>38</sup> 274

275 Other HIV protease inhibitors such as darunavir and ritonavir  
276 were selected by one of the models, but failed for the other. 276

**Table 2. Results of the VS Campaign on the Homology Model of SARS-CoV-2 M<sup>pro</sup> (QHD43415)<sup>a,b</sup>**

Drug Name	Dock score	Nwat-MMGBSA <sup>c,d</sup>
Casposfungin	<b>-108.3</b>	-97.9 ± 12.4
Lopinavir	<b>-106.5</b>	-89.9 ± 5.9
Atazanavir	<b>-109.9</b>	-86.0 ± 7.0
GHRP-2	<b>-116.7</b>	-79.2 ± 11.1
Indinavir	<b>-105.4</b>	-78.6 ± 6.5
Angiotensin II	<b>-125.7</b>	-75.7 ± 9.2
Dehydroandrographolide Succinate	<b>-99.4</b>	<b>-61.1</b>
Ritonavir	-112.3	-58.3 ± 7.8
Azilsartan medoxomil	-102.1	-54.4
Salvianolic acid B	-116.0	-51.0 ± 7.7
Vilanterol	-100.7	-50.9
Elbasvir	-110.2	-48.0 ± 7.7
Clindamycin	-99.6	-47.8
Montelukast	-110.1	-47.5 ± 6.9
Latanoprost	-101.0	-46.8
Cobicistat	-119.3	-45.4 ± 11.6
Octenidine	-104.8	-43.6
Mupirocin	-98.1	-42.3
Tyloxapod	-105.5	-41.1 ± 8.3
Echinacoside	-103.1	-40.0
Salmeterol Xinafoate	-105.3	-37.9 ± 7.3
Ledipasvir	-101.5	-37.3
Thonzonium Bromide	-99.3	-36.7
Lomitapide	-98.1	-34.2
Travoprost	-99.2	-34.0
Itraconazole	-100.2	-32.6
Penfluridol	-106.2	-31.8 ± 9.6
Cisatracurium besylate	-100.3	-23.6
Retinol palmitate	-100.1	-21.8
Terfenadine	-98.1	-17.7

<sup>a</sup>The homology model of SARS-CoV-2 M<sup>pro</sup> was made available by the Zhang group at <https://zhanglab.cmb.med.umich.edu/C-I-TASSER/2019-nCov/>. <sup>b</sup>Top 2% of compounds selected from the docking of 3118 FDA approved drugs and rescored by Nwat-MMGBSA (Nwat = 30) are shown. Compounds that ranked better than the reference are highlighted in bold. The 4MDS crystallographic ligand in complex with SARS-CoV 3CLpro, a close homologue of SARS-CoV-2 M<sup>pro</sup>, was used to compute reference scorings. Docking and Nwat-MMGBSA scores are -96.4 and -59.8 ± 5.3 kcal/mol, respectively. <sup>c</sup>Nwat-MMGBSA rescoring was done considering 30 explicit water molecules around the ligand (Nwat = 30).

277 Indeed, darunavir scored rather well within 6LU7 screening, 278 while ritonavir was high-ranked by QHD43415 although the 279 Nwat-MMGBSA score was slightly lower than the chosen 280 thresholds for both compounds. Interestingly, similar results 281 were also obtained by another group using artificial 282 intelligence.<sup>39</sup> However, ritonavir alone showed an EC<sub>50</sub> greater 283 than 100 μM in Vero E6 cells.<sup>38</sup>

284 Although some clinical studies on the use of HIV protease 285 inhibitors in COVID-19 were already terminated when this 286 screening was made, their results were not already available 287 (<https://clinicaltrials.gov/ct2/results?cond=COVID-19>). 288 Now, a publication showing that a combination of lopinavir and 289 ritonavir succeeded in alleviating symptoms and shortening the 290 hospitalization in patients with mild to moderate COVID-19, 291 especially when used in association with ribavirin.<sup>40</sup> Never- 292 theless, it should also be noted that no benefits were observed for 293 hospitalized patients with severe COVID-19 when treated with 294 lopinavir-ritonavir, beyond standard care,<sup>41</sup> suggesting that the

treatment is only effective when given at an early stage of the 295 disease. Cobicistat, another drug that is approved for the 296 treatment of HIV infection, has been selected by the VS on the 297 6LU7 receptor model as a potential M<sup>pro</sup> inhibitor, even if its 298 main mechanism is claimed to be the inhibition of CYP3A.<sup>42</sup> At 299 the moment, a combination of darunavir and cobicistat is under 300 clinical evaluation for COVID-19, but preliminary results on 301 efficacy and safety are not encouraging. However, final results 302 are expected for August 31st, 2020.<sup>43</sup> 303

Some drugs already approved for the treatment of hepatitis C 304 were also identified. These includes elbasvir,<sup>44</sup> ledipasvir,<sup>45</sup> and 305 velpatasvir,<sup>46</sup> that were also identified in other *in silico* 306 screenings.<sup>19,47</sup> Notably, clinical trials to evaluate the efficacy 307 of ledipasvir on COVID-19 are currently ongoing ([https://](https://clinicaltrials.gov/ct2/results?cond=COVID-19) 308 [clinicaltrials.gov/ct2/results?cond=COVID-19](https://clinicaltrials.gov/ct2/results?cond=COVID-19)). 309

Interestingly, angiotensin II and GHRP-2 are selected in both 310 screenings. Since the M<sup>pro</sup> catalytic activity is to cleave the 311 polypeptide, a peptide of about 15 amino acids, it is plausible that 312 peptides, such as angiotensin II and GHRP-2 of 8 and 6 amino 313 acids, respectively, can fit into the M<sup>pro</sup> active site. Although the 314 use of these hormones might not be indicated for the treatment 315 of SARS-CoV-2, their structures might be used as templates for 316 further drug development. Similarly, the antibiotic polymyxin B 317 was also picked as a high-rank hit, although by the 6LU7 model 318 only, probably due to its peptide nature. Interestingly, 319 polymyxin B was top-ranked within the S-protein screening 320 also, as discussed later in this article. Another lipopeptide, 321 caspofungin, has also been identified, but by the QHD43415 322 model only. Caspofungin is an antifungal drug specifically used 323 in HIV-infected individuals.<sup>49</sup> It was also identified in another 324 independent study as an inhibitor of SARS-CoV-2 replication,<sup>50</sup> 325 even if the Nsp12 polymerase has been claimed as the target. 326

A hit that might be worthy of attention, although only 327 identified by the QHD43415 model, is dehydroandrographolide 328 succinate (DAS). DAS is a natural product extracted from 329 *Andrographis paniculate*, well-known by traditional Chinese 330 medicine.<sup>51</sup> Indeed, while the herb has long been used to treat 331 cold and fever, purified andrographolides, including DAS and 332 analogues, have been prepared and used to treat respiratory 333 diseases.<sup>52,53</sup> Antibacterial, antiviral, anti-inflammatory, and 334 immune-stimulatory activities were claimed for DAS,<sup>54</sup> 335 including the inhibition of HIV and H5N1 viruses *in vitro*.<sup>55,56</sup> 336

Several other compounds were selected by initial docking but 337 failed during the MD simulation phase (Tables S2 and S3). Such 338 a failure might be due to several causes, among all poor 339 parametrization (the BCC charge parametrization method,<sup>57</sup> 340 instead of the more rigorous RESP method,<sup>58</sup> was chosen for 341 time constraints). However, the reason for the failure might also 342 be due to severe steric clashes or mispositioning during the 343 docking stage. Thus, although some good hits might be found 344 within the “F” series, these selections are to be considered as the 345 least reliable. 346

### Virtual Screening on Spike Protein 347

When this work was realized, no S-protein RBD-targeting small 348 molecule was known either for SARS-CoV-2 or other 349 coronaviruses. Conversely, few antibodies recognizing the 350 RBD<sup>59–62</sup> and a recombinant ACE2 enzyme<sup>63</sup> are reported. In 351 addition, a 23-mer peptide derived from the ACE2 showed an 352 affinity of 47 nM toward the SARS-CoV-2 RBD,<sup>64</sup> and a few 353 other peptides were developed to inhibit the interactions of the 354 S2 subunit during the fusion process in both SARS-CoV and 355 SARS-CoV-2.<sup>65</sup> Nonetheless, considering that several com- 356

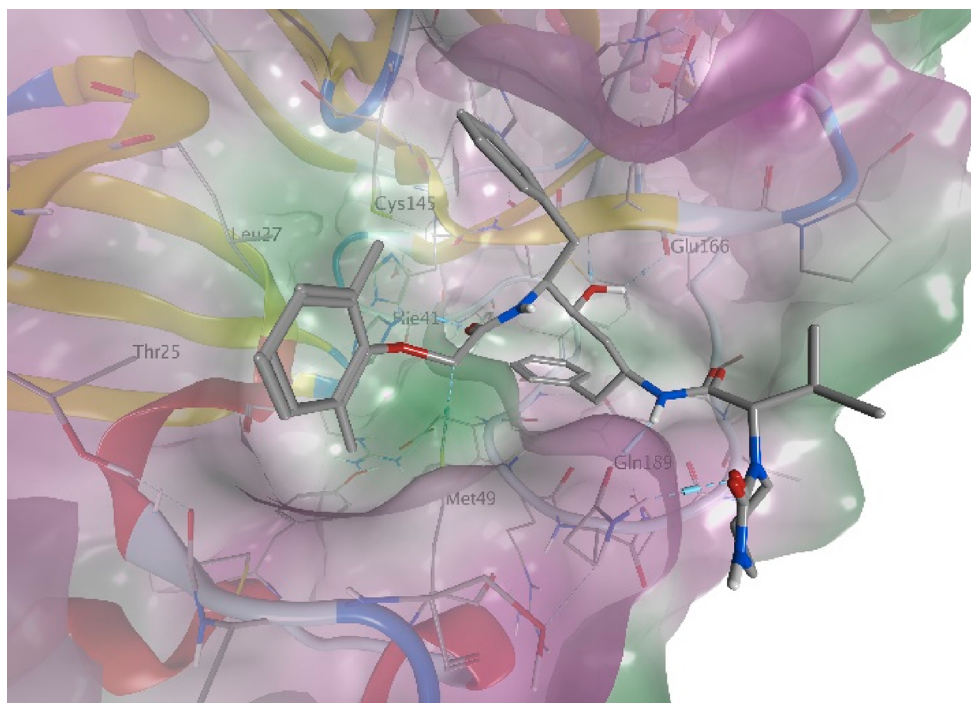


**Figure 1.** Predicted binding mode of lopinavir to  $M^{pro}$ . The model was obtained by performing a cluster analysis of the MD trajectory of the docking pose, followed by a backbone-restrained geometry minimization of the main cluster using MOE.

357 pounds that are currently being tested, some with positive  
358 results, were identified by our VS campaign on  $M^{pro}$ , the results  
359 reported hereafter can also represent a step toward the  
360 treatment against SARS-CoV-2.

### 361 RBD Binding Sites Definition

362 As for most of the protein–protein interaction (PPIs)  
363 interfaces,<sup>66</sup> the one between hACE2 and RBD is quite  
364 extended. However, it is possible to target only the residues  
365 making the major contribution to the binding free energy  
366 between the two proteins (hot spots). In light of this, an alanine  
367 scanning analysis was performed by individually mutating the  
368 RBD residues at the interface with hACE2 (see [Methods](#), [Figure](#)  
369 [2](#) and [Table S4](#)), in order to determine which are the RBD hot

spot residues. This allowed us to define two clusters of hot spots  
([Figures 2](#) and [3](#)), in agreement with a recently published  
preprint article.<sup>67</sup> More in detail, the first cluster (cluster 1)  
involves Leu455, Phe456, Phe486, Asn487, Tyr489, and  
Gln493, while the second one (cluster 2) includes Tyr449,  
Gln498, Thr500, Asn501, and Tyr505 ([Figures 2](#) and [3](#)). It has  
to be noted that the found hot spots are not included in the  
observed mutations found so far,<sup>68</sup> suggesting that they can be  
safely targeted by potential inhibitors of the ACE2-RBD  
interaction.

In the second cluster we can find Gln498: when it is mutated  
to alanine, the complex  $\Delta G$  has a loss of  $\sim 9$  kcal/mol, indicating  
that this residue is fundamental for the interaction with hACE2.  
Indeed, the Gln498 side chain is involved in a highly stable H-  
bond (occupancy  $>80\%$ , [Table S2](#)) with the hACE2 Asp38 side  
chain, and for the remaining  $\sim 20\%$  it interacts with the hACE2  
Lys353 side chain.

Since cluster 1 and 2 are well separated and localized at the  
two extremities of the RBD interface to hACE2, it is possible to  
determine two distinct binding sites to target by VS (see  
[Methods](#)), called BS1 and BS2, respectively, in the following  
discussion. Working with two different possible RBD binding  
sites represents an advantage as compared to other similar  
studies, where a single but larger binding site on the RBD was  
defined.<sup>18,69</sup> Indeed, as previously said, most of the currently  
available drugs are small molecules which are able to interact  
with a limited surface and only with a few residues. Therefore,  
selecting two binding sites corresponding to specific hot spot  
clusters makes the docking pose search more efficient, by  
limiting the search space. In addition, it allows us to discard  
molecules which are predicted to strongly interact with the  
protein target but on a protein region without hot spots, not  
assuring the PPI inhibition.

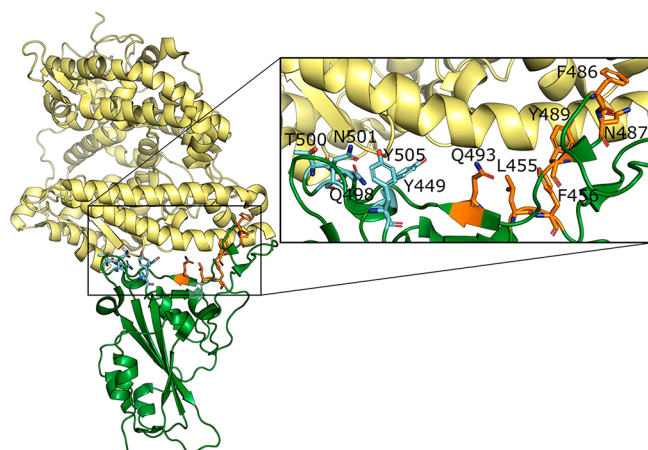


**Figure 2.** Complex between hACE2 (yellow) and SARS-CoV-2 RBD (green) from the X-ray structure (PDB code 6M0J). The hot spot residues are represented in sticks and labeled in the inset. Hot spots of cluster 1 are represented in orange, while those of cluster 2 are represented in cyan.

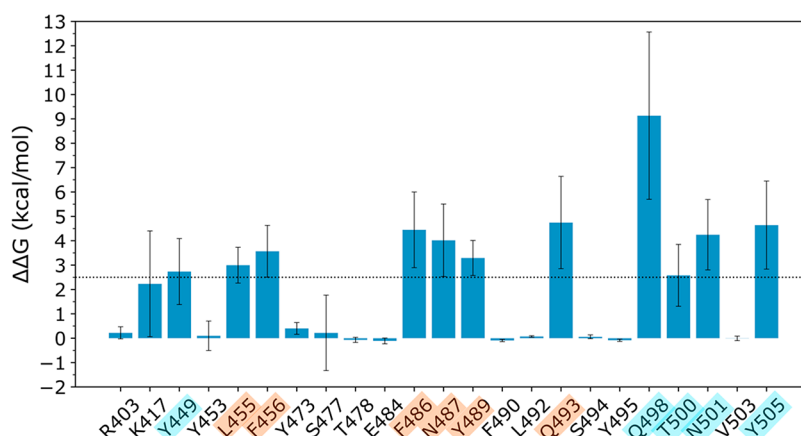


**Figure 3.** Difference in the binding free energy between the mutated system and the native one computed on the last 10 ns of the MD simulation of the hACE2-RBD complex. All the residues for which the  $\Delta\Delta G$  is greater than the threshold (2.5 kcal/mol) have been considered as hot spots. The hot spots of cluster 1 are highlighted in orange and those of cluster 2 in cyan.

**Table 3. Results of the VS Campaign on the Crystal Structure of SARS-CoV-2 S-Protein RBD Binding Site 1<sup>a</sup>**

Drug name	Dock score	Nwat-MMGBSA <sup>b</sup>	Drug name	Dock score	Nwat-MMGBSA <sup>b</sup>
Polymyxin B	-107.6	-152.1 ± 11.5	Ginsenoside Rb1	-96.2	-64.2 ± 10.9
Colistin	-101.7	-149.4 ± 12.5	Somatostatin	-98.6	-61.2 ± 10.2
Daptomycin	-95.2	-137.8 ± 13.1	Ledipasvir	-97.4	-60.8 ± 8.5
Oritavancin	-93.6	-126.8 ± 13.3	Zafirlukast	-91.0	-57.7 ± 6.0
Thymopentin	-92.4	-121.9 ± 14.6	Latanoprost	-98.0	-56.5 ± 7.4
Terlipressin	-103.7	-118.0 ± 9.6	Fexofenadine	-91.0	-53.3 ± 17.9
Lypressin	-103.2	-111.3 ± 12.6	Velpatasvir	-91.3	-53.1 ± 8.7
Vancomycin	-96.2	-104.6 ± 17.9	Nebivolol	-90.9	-52.2 ± 7.5
Leuprolide	-110.7	-101.3 ± 10.8	Azelnidipine	-91.1	-51.6 ± 7.6
Alarelin	-104.6	-98.3 ± 8.9	Astemizole	-91.9	-51.1 ± 5.5
Deferoxamine	-90.8	-97.4 ± 9.0	Pranlukast	-91.5	-50.3 ± 5.6
Bacitracin	-93.9	-97.0 ± 11.8	Travoprost	-89.9	-49.1 ± 8.5
Senoside B	-91.3	-94.9 ± 8.9	Vilazodone	-97.0	-48.6 ± 5.9
Angiotensin II human	-104.2	-94.8 ± 11.6	Acidinium	-90.0	-48.5 ± 6.4
Salvianolic acid B	-104.5	-93.9 ± 10.2	Octenidine	-102.4	-48.1 ± 9.5
Gonadorelin	-104.2	-93.5 ± 8.7	Elbasvir	-97.4	-47.8 ± 10.0
Nafarelin	-111.8	-90.3 ± 11.5	L-Ascorbyl 6-palmitate	-90.8	-47.7 ± 8.0
Amphotericin B	-108.0	-89.2 ± 11.8	Silodosin	-90.3	-47.1 ± 9.2
Madecassoside	-96.0	-88.5 ± 10.2	Ponatinib	-96.6	-44.6 ± 7.7
Micafungin	-95.6	-86.0 ± 12.4	Ebastine	-95.2	-44.3 ± 7.9
Mupirocin	-91.4	-82.1 ± 7.0	Vitamin K2	-95.7	-41.5 ± 6.1
Goserelin	-107.9	-81.0 ± 12.7	Posaconazole	-99.5	-32.6 ± 7.7
Nystatin	-102.2	-78.8 ± 12.8	Penfluridol	-90.3	-31.5 ± 9.1
Echinacoside	-93.2	-71.9 ± 9.5	Vitamin A	-96.6	-31.1 ± 8.1
Dalbavancin	-90.7	-69.7 ± 12.5	Lapatinib	-100.8	-31.1 ± 7.2
Tyloxapol	-106.6	-68.5 ± 7.7	Behenic alcohol	-93.4	-28.8 ± 7.2
Icatibant	-115.8	-67.9 ± 10.4	Gefarnate	-89.8	-26.2 ± 10.4
Landirolol	-91.6	-67.3 ± 12.4	Azilsartan	-90.2	-24.5 ± 12.4
Venetoclax	-92.5	-66.9 ± 7.3			
Vilanterol	-95.1	-65.5 ± 8.7			
Montelukast	-97.6	-65.3 ± 11.9			
Salmeterol	-100.4	-64.6 ± 7.5			

<sup>a</sup>Top 2% of compounds selected from the docking of 3118 FDA approved drugs and rescored by Nwat-MMGBSA (Nwat = 60) are shown ranked by Nwat-MMGBSA scores. <sup>b</sup>Energy obtained by using Nwat = 60, ± standard deviation.

### 403 Virtual Screening on RBD-BS1

404 The results of the VS are reported in Table 3, after the deletion  
405 of those molecules which, although being part of the top 2%  
406 during the docking step, left the binding during the MD  
407 simulation (namely, GHRP-2, cobicistat, oxytocin, and vitamin  
408 B12). Although different Nwat values have been evaluated, we  
409 will limit our discussion to the results provided by Nwat-

MMGBSA with Nwat = 60, since this value resulted to be  
appropriate when dealing with PPI inhibitors.<sup>20,34</sup>

It is not surprising that the best ranked ligands are peptide-like  
molecules, since these are usually larger than small molecules  
and allow a better interaction with the PPI binding partner. Most  
of the top ranked peptide-like molecules, such as the polymyxin  
B, colistin, and daptomycin, are currently used as antibiotics  
because of their ability in disrupting the bacterial membrane.

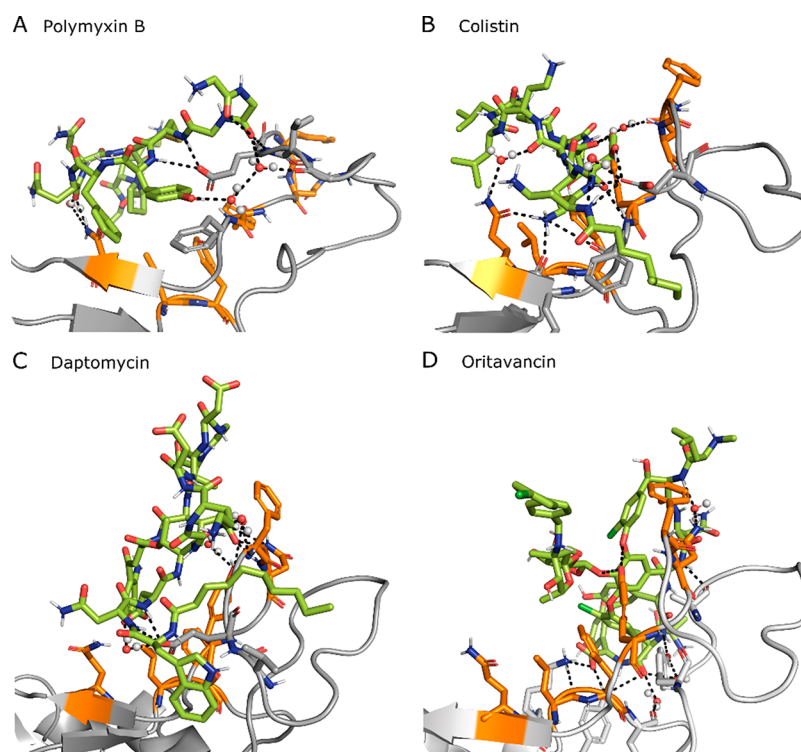


**Figure 4.** Snapshot of the MD simulation between RBD (gray) and one of the top four ligands (green). RBD BS1 hot spots are highlighted in orange. Direct and water (spheres) mediated H-bonds are also displayed as dashed lines. Additional RBD residues interacting with the ligand are displayed as sticks.

418 Among these, polymyxin B has been tested within a compas-  
419 sionate use protocol for patients with an immediately life-  
420 threatening condition.<sup>70</sup>

421 Others compounds identified herein as potential binders of  
422 the S-protein are terlipressin and lypressin, analogs of vaso-  
423 pressin and used against hypotension. We can also find  
424 hormone-peptides, such as alarelin or leuporelin, which belong  
425 to the gonadotropin-releasing hormone family, or somatostatin,  
426 an endocrine system regulator. Furthermore, we can observe the  
427 presence of peptidomimetics, such as icatibant, which acts as an  
428 antagonist of B2 bradykinine receptors. This last compound was  
429 also identified by an independent study as a potential disruptor  
430 of the Spike-ACE2 PPI.<sup>71</sup>

431 The only nonpeptide molecules found in the top 2% are large  
432 compounds (molecular weight >500 g/mol) rich in H-bond  
433 acceptor and donor atoms. This is not surprising, indeed it has  
434 been suggested that the SARS-CoV-2 binds to the host heparan  
435 sulfate chains of the heparan sulfate proteoglycan receptor also,  
436 initiating the internalization.<sup>72</sup> In addition, it has been recently  
437 shown that the RBD can bind to the heparin<sup>73–75</sup> and that an  
438 octosaccharide sequence strongly inhibits this interaction ( $IC_{50}$   
439 = 38 nM).<sup>73</sup> In our VS campaign, we found the salvianolic acid B  
440 (also found in  $M^{pro}$  screening), used as antioxidant, antifungal  
441 drugs (amphotericin B, micafungin, nystatin, micafungin), the  
442 madecassoside and ginsenoside Rb1, molecules with anti-  
443 inflammatory properties, and the tensioactive tyloxapol in the  
444 top 2%. Interestingly, a combination of amphotericin B and  
445 deoxycholate was shown to have an effect in decreasing the  
446 infectivity of transmissible gastroenteritis coronavirus.<sup>76</sup> We also  
447 found at #11 deferoxamine, a chelating agent under clinical  
448 study against COVID-19 (ClinicalTrials.gov Identifier:  
449 NCT04333550). However, this molecule is claimed as  
450 responsible of chelating the iron whose dissociation from

heme is increased by SARS-CoV-2, causing oxidative stress and  
451 damage to the lung.<sup>77</sup> The top 2% also contains antivirals such as  
452 ledipasvir and elbasvir, used against hepatitis C. However, their  
453 mechanism of action involves the inhibition of viral proteins.  
454 Additionally, both elbasvir and ledipasvir were identified on the  
455 same target in another independent study, using a different  
456 computational protocol.<sup>47,48</sup>

457 Unexpectedly, among the best 60 RBD ligands there is  
458 salmeterol and vilanterol, which are agonists of  $\beta_2$ -adrenergic  
459 receptors, a class of molecules which showed a minor  
460 amplification of the viral phenotype in a recent preprinted  
461 study.<sup>78</sup> Conversely, another antiasthmatic drug, montelukast,  
462 has been shown to cause the disruption of the viral integrity of  
463 the Zika virus;<sup>79</sup> thus, its presence in the top 2% (#39) enhances  
464 the interest of this compound against SARS-CoV-2 also.  
465

466 In addition, we also found a few beta-adrenergic blockers,  
467 namely landiolol and nebivolol; this class of molecules, although  
468 it is not known to bind to the S-protein, has been hypothesized  
469 to be able to decrease the SARS-CoV-2 entry into the cells by  
470 downregulating ACE2 receptors.<sup>78,80</sup>

471 Peptides are usually highly flexible and require an extensive  
472 conformational sampling before the VS procedure. However,  
473 most of the peptides herein considered are partially cyclic: this  
474 creates a structural constraint, making feasible and globally  
475 reliable their docking to RBD.

476 The best scored compounds interact with the RBD through  
477 hydrophobic interactions and stable direct and water-mediated  
478 H-bond with BS1 hot spots and neighboring residues, creating a  
479 stable network of interactions, as shown in Figure 4 for the four  
480 top-ranked ligands. For example, polymyxin B can create direct  
481 H-bonds with Glu484, Phe486, Asn487, Tyr489, and Gln493  
482 and water-mediated H-bonds with Asn487, Glu484, and

Table 4. Results of the VS Campaign on the Crystal Structure of SARS-CoV-2 S-Protein RBD Binding Site 2<sup>4</sup>

Drug name	Dock score	Nwat-MMGBSA (nwat = 60) ± standard deviation	Drug name	Dock score	Nwat-MMGBSA (nwat = 60) ± standard deviation
Polymyxin B	-99.4	-164.3 ± 11.3	Elbasvir	-108.7	-73.4 ± 7.3
Thymopentin	-97.7	-154.5 ± 12.9	Manidipine	-92.6	-72.3 ± 6.4
Icatibant	-107.6	-143.1 ± 12.0	Ginsenoside Rb1	-93.8	-72.3 ± 10.8
Octreotide	-94.6	-127.2 ± 10.9	Lercanidipine	-95.5	-71.3 ± 6.5
Oritavancin	-98.3	-123.6 ± 14.1	Atazanavir	-98.1	-70.8 ± 7.4
Nystatin	-110.8	-123.2 ± 10.5	Cobicistat	-100.3	-69.5 ± 8.7
Terlipressin	-98.2	-122.8 ± 10.7	Montelukast	-100.8	-67.5 ± 7.6
Salvianolic acid B	-112.0	-121.6 ± 10.6	Vitamin B12	-93.5	-65.9 ± 11.7
Echinacoside	-104.6	-113.3 ± 8.2	Tyloxapol	-104.1	-64.5 ± 7.1
Bleomycin	-103.4	-110.1 ± 15.3	Micafungin	-95.4	-63.2 ± 12.7
Angiotensin II human	-100.3	-107.3 ± 12.1	Salmeterol	-99.8	-62.8 ± 8.6
Nafarelin	-121.9	-106.4 ± 10.6	Zafirlukast	-94.6	-61.8 ± 5.8
Leuprorelin	-114.5	-106.2 ± 9.8	Labetalol	-91.8	-61.4 ± 5.9
Senoside B	-91.9	-99.1 ± 10.6	Indinavir	-105.0	-60.0 ± 8.7
Aliskiren	-99.6	-96.3 ± 6.7	Latanoaprost	-94.7	-57.2 ± 6.5
Caspofungin	-99.1	-95.4 ± 14.3	Amphotericin B	-132.7	-57.0 ± 7.8
Alarelin	-103.7	-94.6 ± 10.3	Ombitasvir	-94.3	-53.2 ± 12.6
GHRP-2	-104.9	-93.8 ± 9.9	Tocofersolan	-91.6	-52.5 ± 6.8
Lentinan	-96.5	-93.4 ± 12.5	Haloperidol	-91.9	-52.5 ± 9.2
Leuprolide	-109.6	-93.4 ± 11.1	Tafuprost	-94.3	-51.6 ± 6.3
Hederacoside C	-98.5	-89.1 ± 10.1	Itraconazole	-96.0	-46.5 ± 7.3
Gonadorelin	-111.4	-88.8 ± 13.0	Avanafil	-96.7	-46.2 ± 5.8
Pneumocandin	-95.3	-86.4 ± 11.4	Ledipasvir	-92.6	-43.4 ± 8.2
Daptomycin	-94.4	-85.4 ± 18.5	Octenidine	-99.1	-43.2 ± 9.1
NAD+	-96.9	-83.6 ± 33.4	Thonzonium	-92.4	-41.0 ± 8.1
Deferoxamine	-97.2	-83.3 ± 8.5	Fulvestrant	-96.5	-40.9 ± 7.1
Goserelin	-99.2	-80.4 ± 10.9	Gefarnate	-91.7	-39.3 ± 6.6
Neohesperidin	-94.2	-79.8 ± 8.0	Clindamycin	-91.9	-33.4 ± 7.8
Gramicidin	-98.5	-79.3 ± 11.8			
Somatostatin	-110.7	-77.2 ± 10.7			
Vilanterol	-96.3	-75.5 ± 6.3			
Desmopressin	-95.1	-74.9 ± 11.7			

<sup>4</sup>Top 2% of compounds selected from the docking of 3118 FDA approved drugs and rescored by Nwat-MMGBSA (Nwat = 60) are shown ranked by Nwat-MMGBSA scores.

483 Phe490. In addition, we can observe hydrophobic interactions  
484 between polymyxin B and Val483 and Phe486.

#### 485 Virtual Screening on RBD-BS2

486 Similar results were obtained for the BS2, as shown in Table 4. In  
487 this case also, the ligands which left the binding site during the  
488 MD simulation, namely colistin, ritonavir, salmeterol, dalba-  
489 vancin, and atazanavir, were removed from the list. It is  
490 interesting to notice that colistin was the second best ligand for  
491 BS1; conversely for BS2, even if the docking procedure ranked  
492 this ligand in the top 2%, it could not maintain the favorable  
493 interactions during the MD simulation. This highlights the  
494 importance of performing MD simulations on the complexes  
495 obtained by the docking procedure and provides a further  
496 confirmation of the quality of our protocol.<sup>20</sup> In addition,  
497 although the amino acid composition of the two binding sites is  
498 quite similar (Figure 2), their conformational organization is  
499 specific and exploitable for further studies on the development of  
500 new potential inhibitors of the RBD-hACE2 interaction.

501 Globally, the top 2% of ligands binding to BS2 is similar in  
502 composition to the one binding to BS1: most of the ligands are  
503 peptide-like molecules known to be antibiotics, antifungals,  
504 peptide hormones, and pressure regulators. As noticed for BS1,  
505 we can also find molecules containing both large hydrophobic  
506 groups and H-bond donors and acceptors, such as echinacoside  
507 and aliskiren (Table 4). The best ranked ligand poses show a

tight network of direct and water-mediated H-bonds with both  
the hot spot residues and the neighboring ones, in addition to  
additional hydrophobic interactions (Figure 5). For example,  
the best ranked molecule, which is polymyxin B also in this case,  
creates direct H-bonds with Arg403, Tyr449, Gly496, the most  
relevant hot spot Gln498, and Asn501, together with water-  
mediated H-bonds with Glu406, Tyr449, Tyr453, Gln493,  
Gln498, and Thr500. Except for polymyxin B, the ranking is  
quite different from that for BS1, with molecules which were not  
present in the top 10 for BS1 being ranked in the top positions  
for BS2, such as icatibant (#3) and octeotide (#4).

Thymopentin is the only linear peptide found in the top 2%  
docked molecules for both BS. In order to verify if the docked  
conformation properly took into account for the peptide  
flexibility and its accessible conformations, we predicted the  
3D structure of the peptide using the PEPFOLD3<sup>81</sup> server, and  
the best model has a backbone RMSD of 1.3 Å (Figure S2) from  
the thymopentin docked to RBD and ranked second in the VS  
campaign targeting RBD BS2. It should be underscored that  
thymopentin is an immunostimulant peptide applied in  
numerous clinical studies during the AIDS pandemic between  
1983 and 1985.<sup>82,83</sup> Therefore, together with the good binding  
to the SARS-CoV-2 S-protein RBD shown within this VS  
campaign, a potential immunostimulant effect of this peptide

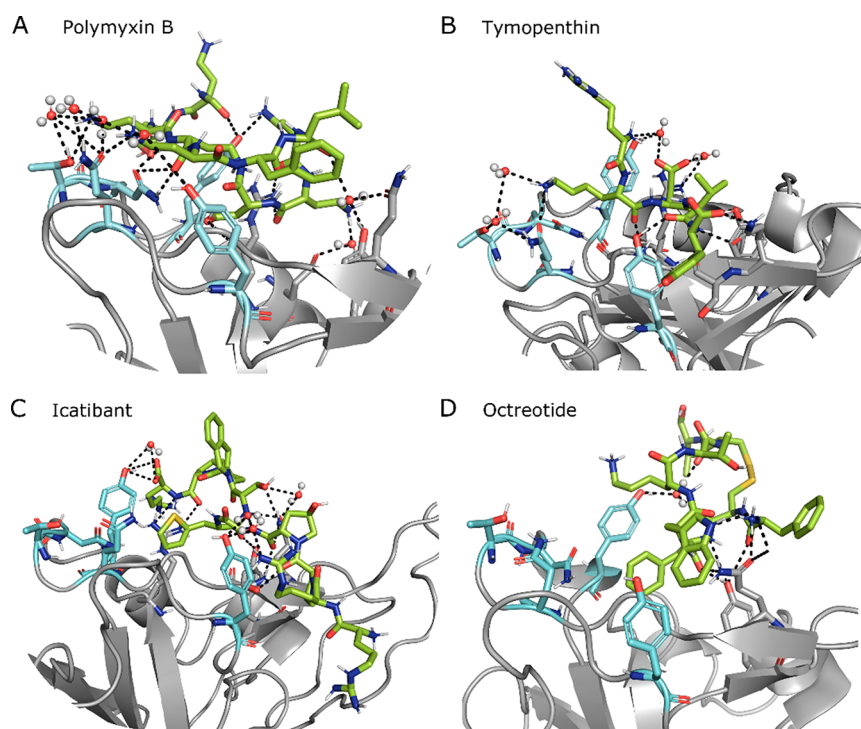


**Figure 5.** Snapshot of the MD simulation between RBD (gray) and one of the top four ligands (green). RBD BS2 hot spots are highlighted in cyan. Direct and water (spheres) mediated H-bonds are also displayed as dashed lines. Additional RBD residues interacting with the ligand are displayed as sticks.

532 could be helpful in enhancing the immune response to the viral  
533 infection.

## 534 ■ CONCLUSIONS

535 SARS-CoV-2 currently represents a major threat to human  
536 health, having caused hundreds of thousands of deaths in a few  
537 months. At the moment a cure against this pandemic infection is  
538 still lacking, together with a vaccine against this virus. In order to  
539 rapidly face the emergency, testing the efficacy against SARS-  
540 CoV-2 of drugs already approved for the treatment of other  
541 diseases (drug repurposing) is a good option. Indeed, it has the  
542 advantage of exploiting molecules which have already been  
543 tested in terms of toxicity and which are usually easy to purchase  
544 for clinical tests and patient administration. Therefore, positive  
545 results from this kind of procedure can speed up the process of  
546 finding a treatment against SARS-CoV-2. However, the number  
547 of approved drugs by the major jurisdictions is huge and directly  
548 performing either *in vitro* or *in vivo* studies on all of them would  
549 be time-consuming; thus a fundamental contribution to  
550 accelerate the screening can come from *in silico* techniques.

551 Within this context, we proposed a multiple VS campaign  
552 aimed to prioritize the testing against SARS-CoV-2 of already  
553 approved molecules. More in detail, we performed 4  
554 independent VS procedures of more than 3000 approved  
555 drugs using two different SARS-CoV-2 proteins: the main  
556 proteinase M<sup>Pro</sup> and the RBD of the S-protein. Inhibiting the  
557 former would block the viral replication, while targeting the S-  
558 protein domain (i.e., RBD) would hamper the viral entry into  
559 the human cells. We applied an advanced VS procedure, which  
560 already proved to better discriminate between active and  
561 inactive compounds on multiple systems, compared to standard  
562 docking procedures.<sup>20</sup>

563 The VS campaign against M<sup>Pro</sup> ranked in the top 2% of  
564 inhibitors of the HIV protease, such as indinavir, atazanavir, and

lopinavir, which recently proved to be able to alleviate the  
565 symptoms of mild-to-moderate SARS-CoV-2 infection in  
566 combination with ritonavir.<sup>40</sup>

567  
568 The VS campaign on Spike protein RBD indicated that  
569 peptides or peptidomimetics actually used as antibiotics (i.e.,  
570 polymyxin B, colistin, and daptomycin), pressure regulators (i.e.,  
571 terlipressin and lypressin), hormone-peptides (i.e., alarelin and  
572 leuporelin), and immunostimulants, such as the thymopentin,  
573 could be evaluated against SARS-Cov-2 also. Currently, there  
574 are not clinical studies on molecules known to specifically  
575 disrupt the interaction between the human ACE2 and the RBD;  
576 however, a few peptides were designed with this aim and  
577 successfully tested *in vitro*, validating our hypothesis that  
578 peptide-based molecules can be adapted to inhibit the ACE2-  
579 RBD interaction.

580 In conclusion, together with providing a good starting point  
581 for future *in vitro* and *in vivo* investigations on the resulting top  
582 compounds, the results of this extensive VS can support the  
583 design of selective and specific molecules to treat SARS-CoV-2  
584 infection by targeting different viral proteins.

## 585 ■ ASSOCIATED CONTENT

### 586 ■ Supporting Information

587 The Supporting Information is available free of charge at  
588 <https://pubs.acs.org/doi/10.1021/acs.jproteome.0c00383>.

589 Figure S1. RMSD of the RBD-hACE2 complex backbone  
590 atoms from the X-ray structure during the MD simulation.  
591 Table S1. Difference in the binding free energies between  
592 the mutated and the native RBD-hACE2 complex  
593 obtained from the alanine scanning. Table S2. Com-  
594 pounds selected by docking on M<sup>Pro</sup> (6LU7 model) that  
595 failed during the MD/Nwat-MMGBSA rescoring step.  
596 Table S3. Compounds selected by docking on M<sup>Pro</sup>

597 (QHD43415 homology model) that failed during the  
598 MD/Nwat-MMGBSA rescoring step. Table S4. Hydro-  
599 gen bonds between RBD and hACE2 during the last half  
600 of the 20 ns MD simulation. Figure S2. Superposition of  
601 thymopentin docked to RBD BS2 and the PEPFOLD3  
602 structure prediction. (PDF)

## 603 ■ AUTHOR INFORMATION

### 604 Corresponding Authors

605 **Irene Maffucci** – Université de technologie de Compiègne, UPJV,  
606 CNRS, Enzyme and Cell Engineering, 60 203 Compiègne Cedex,  
607 France; Email: irene.maffucci@utc.fr

608 **Alessandro Contini** – Università degli Studi di Milano,  
609 Dipartimento di Scienze Farmaceutiche, Sezione di Chimica  
610 Generale e Organica "A. Marchesini", 21 20133 Milano, Italy;  
611 [orcid.org/0000-0002-4394-8956](https://orcid.org/0000-0002-4394-8956);  
612 Email: alessandro.contini@unimi.it

613 Complete contact information is available at:

614 <https://pubs.acs.org/10.1021/acs.jproteome.0c00383>

### 615 Author Contributions

616 The manuscript was written through contributions of all  
617 authors. All authors have given approval to the final version of  
618 the manuscript. All the authors contributed equally.

### 619 Funding

620 No specific funding was received for this work.

### 621 Notes

622 The authors declare no competing financial interest.

## 623 ■ ACKNOWLEDGMENTS

624 A.C. thanks Dr. Andrea Bazzoli for useful discussions that lead to  
625 the idea of performing a screening on M<sup>Pro</sup>.

## 626 ■ ABBREVIATIONS

627 VS, virtual screening; MD, molecular dynamics; RBD, receptor  
628 binding domain; ACE2, angiotensin converting enzyme 2; H-  
629 bond, hydrogen bond

## 630 ■ REFERENCES

- 631 (1) Walls, A. C.; Park, Y.-J.; Tortorici, M. A.; Wall, A.; McGuire, A. T.;  
632 Velesler, D. Structure, Function, and Antigenicity of the SARS-CoV-2  
633 Spike Glycoprotein. *Cell* **2020**, *181*, 1–12.
- 634 (2) Wrapp, D.; Wang, N.; Corbett, K. S.; Goldsmith, J. A.; Hsieh, C.  
635 L.; Abiona, O.; Graham, B. S.; McLellan, J. S. Cryo-EM Structure of the  
636 2019-NCoV Spike in the Prefusion Conformation. *Science (Washington,*  
637 *DC, U. S.)* **2020**, *367*, 1260–1263.
- 638 (3) Ou, X.; Liu, Y.; Lei, X.; Li, P.; Mi, D.; Ren, L.; Guo, L.; Guo, R.;  
639 Chen, T.; Hu, J.; Xiang, Z.; Mu, Z.; Chen, X.; Chen, J.; Hu, K.; Jin, Q.;  
640 Wang, J.; Qian, Z. Characterization of Spike Glycoprotein of SARS-  
641 CoV-2 on Virus Entry and Its Immune Cross-Reactivity with SARS-  
642 CoV. *Nat. Commun.* **2020**, *11*, 1620.
- 643 (4) Lan, J.; Ge, J.; Yu, J.; Shan, S.; Zhou, H.; Fan, S.; Zhang, Q.; Shi, X.;  
644 Wang, Q.; Zhang, L.; Wang, X. Structure of the SARS-CoV-2 Spike  
645 Receptor-Binding Domain Bound to the ACE2 Receptor. *Nature* **2020**,  
646 *581*, 215–220.
- 647 (5) Shang, J.; Ye, G.; Shi, K.; Wan, Y.; Luo, C.; Aihara, H.; Geng, Q.;  
648 Auerbach, A.; Li, F. Structural Basis of Receptor Recognition by SARS-  
649 CoV-2. *Nature* **2020**, *581*, 221–224.
- 650 (6) Hamming, I.; Timens, W.; Bulthuis, M. L. C.; Lely, A. T.; Navis, G.  
651 J.; van Goor, H. Tissue Distribution of ACE2 Protein, the Functional  
652 Receptor for SARS Coronavirus. A First Step in Understanding SARS  
653 Pathogenesis. *J. Pathol.* **2004**, *203*, 631–637.

(7) Douglas, G. C.; O'Bryan, M. K.; Hedger, M. P.; Lee, D. K. L.; 654  
Yarski, M. A.; Smith, A. I.; Lew, R. A. The Novel Angiotensin- 655  
Converting Enzyme (ACE) Homolog, ACE2, Is Selectively Expressed 656  
by Adult Leydig Cells of the Testis. *Endocrinology* **2004**, *145*, 4703– 657  
4711. 658

(8) Anand, K.; Ziebuhr, J.; Wadhwani, P.; Mesters, J. R.; Hilgenfeld, R. 659  
Coronavirus Main Proteinase (3CLpro) Structure: Basis for Design of 660  
Anti-SARS Drugs. *Science (Washington, DC, U. S.)* **2003**, *300*, 1763– 661  
1767. 662

(9) Zhang, L.; Lin, D.; Sun, X.; Curth, U.; Drosten, C.; Sauerhering, 663  
L.; Becker, S.; Rox, K.; Hilgenfeld, R. Crystal Structure of SARS-CoV-2 664  
Main Protease Provides a Basis for Design of Improved  $\alpha$ -Ketoamide 665  
Inhibitors. *Science (Washington, DC, U. S.)* **2020**, *368*, 409–412. 666

(10) Hilgenfeld, R. From SARS to MERS: Crystallographic Studies on 667  
Coronaviral Proteases Enable Antiviral Drug Design. *FEBS J.* **2014**, 668  
*281*, 4085–4096. 669

(11) Jin, Z.; Du, X.; Xu, Y.; Deng, Y.; Liu, M.; Zhao, Y.; Zhang, B.; Li, 670  
X.; Zhang, L.; Peng, C.; Duan, Y.; Yu, J.; Wang, L.; Yang, K.; Liu, F.; 671  
Jiang, R.; Yang, X.; You, T.; Liu, X.; Yang, X.; Bai, F.; Liu, H.; Liu, X.; 672  
Guddat, L. W.; Xu, W.; Xiao, G.; Qin, C.; Shi, Z.; Jiang, H.; Rao, Z.; 673  
Yang, H. Structure of Mpro from SARS-CoV-2 and Discovery of Its 674  
Inhibitors. *Nature* **2020**, *582*, 289–293. 675

(12) Roy, A.; Kucukural, A.; Zhang, Y. I-TASSER: A Unified Platform 676  
for Automated Protein Structure and Function Prediction. *Nat. Protoc.* 677  
**2010**, *5*, 725–738. 678

(13) Zhang, C.; Zheng, W.; Huang, X.; Bell, E. W.; Zhou, X.; Zhang, Y. 679  
Protein Structure and Sequence Reanalysis of 2019-NCoV Genome 680  
Refutes Snakes as Its Intermediate Host and the Unique Similarity 681  
between Its Spike Protein Insertions and HIV-1. *J. Proteome Res.* **2020**, 682  
*19*, 1351–1360. 683

(14) Wu, F.; Zhao, S.; Yu, B.; Chen, Y. M.; Wang, W.; Song, Z. G.; Hu, 684  
Y.; Tao, Z. W.; Tian, J. H.; Pei, Y. Y.; Yuan, M. L.; Zhang, Y. L.; Dai, F. 685  
H.; Liu, Y.; Wang, Q. M.; Zheng, J. J.; Xu, L.; Holmes, E. C.; Zhang, Y. 686  
Z. A New Coronavirus Associated with Human Respiratory Disease in 687  
China. *Nature* **2020**, *579*, 265–269. 688

(15) Patick, A. K.; Potts, K. E. Protease Inhibitors as Antiviral Agents. 689  
*Clin. Microbiol. Rev.* **1998**, *11*, 614. 690

(16) Cavasotto, C. N.; Orry, A. J. W. Ligand Docking and Structure- 691  
Based Virtual Screening in Drug Discovery. *Curr. Top. Med. Chem.* 692  
**2007**, *7*, 1006–1014. 693

(17) Clark, D. E. What Has Virtual Screening Ever Done for Drug 694  
Discovery? *Expert Opin. Drug Discovery* **2008**, *3*, 841–851. 695

(18) Choudhary, S.; Malik, Y. S.; Tomar, S. Identification of SARS- 696  
CoV-2 Cell Entry Inhibitors by Drug Repurposing Using in Silico 697  
Structure-Based Virtual Screening Approach. *Front. Immunol.* **2020**, *11*, 698  
1664. 699

(19) Chen, Y. W.; Yiu, C. P. B.; Wong, K. Y. Prediction of the SARS- 700  
CoV-2 (2019-NCoV) 3C-like Protease (3CLpro) Structure: Virtual 701  
Screening Reveals Velpatasvir, Ledipasvir, and Other Drug Repurpos- 702  
ing Candidates. *F1000Research* **2020**, *9*, 9. 703

(20) Maffucci, I.; Hu, X.; Fumagalli, V.; Contini, A. An Efficient 704  
Implementation of the Nwat-MMGBSA Method to Rescore Docking 705  
Results in Medium-Throughput Virtual Screenings. *Front. Chem.* **2018**, 706  
*6*, 43. 707

(21) Amaro, R. E.; Baudry, J.; Chodera, J.; Demir, Ö.; McCammon, J. 708  
A.; Miao, Y.; Smith, J. C. Ensemble Docking in Drug Discovery. *Biophys.* 709  
*J. Biophysical Society*, May 22, 2018; pp 2271–2278. 710

(22) Molecular Operating Environment (MOE), 2019.0102; 711  
Chemical Computing Group Inc.: Montreal, 2019. 712

(23) Turlington, M.; Chun, A.; Tomar, S.; Egger, A.; Grum-Tokars, 713  
V.; Jacobs, J.; Daniels, J. S.; Dawson, E.; Saldanha, A.; Chase, P.; Baez- 714  
Santos, Y. M.; Lindsley, C. W.; Hodder, P.; Mesecar, A. D.; Stauffer, S. 715  
R. Discovery of N-(Benzo[1,2,3]Triazol-1-Yl)-N-(Benzyl)- 716  
Acetamido)Phenyl) Carboxamides as Severe Acute Respiratory 717  
Syndrome Coronavirus (SARS-CoV) 3CLpro Inhibitors: Identification 718  
of ML300 and Noncovalent Nanomolar Inhibitors with an Induced-Fit 719  
Binding. *Bioorg. Med. Chem. Lett.* **2013**, *23*, 6172–6177. 720

- 721 (24) Contini, A. Virtual Screening of an FDA Approved Drugs  
722 Database on Two COVID-19 Coronavirus Proteins. *ChemRxiv*  
723 Preprint. **2020**, DOI: 10.26434/Chemrxiv.11847381.V1.
- 724 (25) Anandakrishnan, R.; Aguilar, B.; Onufriev, A. V. H++ 3.0:  
725 Automating PK Prediction and the Preparation of Biomolecular  
726 Structures for Atomistic Molecular Modeling and Simulations. *Nucleic*  
727 *Acids Res.* **2012**, *40*, W537–541.
- 728 (26) Case, D. A.; Ben-Shalom, I. Y.; Brozell, S. R.; Cerutti, D. S.;  
729 Cheatham, T. E., III; Cruzeiro, V. W. D.; Duke, T. A. D. R. E.;  
730 Ghoreishi, D.; Gilson, M.K.; Gohlke, H.; Goetz, A. W.; Greene, D.;  
731 Harris, R.; Homeyer, N.; Izadi, Y. H. S.; Kovalenko, A.; Kurtzman, T.;  
732 Lee, T. S.; LeGrand, S.; Li, P.; Lin, C.; Liu, J.; Luchko, T.; Luo, R.; D. J.,  
733 Mermelstein, Merz, K. M.; Miao, Y.; Monard, G.; Nguyen, C.; Nguyen,  
734 H.; Omelyan, I.; Onufriev, A.; Pan, F.; R., Qi, Roe, D. R.; Roitberg, A.;  
735 Sagui, C.; Schott-Verdugo, S.; Shen, J.; Simmerling, C. L.; Smith, J.;  
736 SalomonFerrer, R.; Swails, J.; Walker, R. C.; Wang, J.; Wei, H.; Wolf, R.  
737 M.; Wu, X.; Xiao, L.; D. M., Y.; P. A., K. AMBER 2018; University of  
738 California, San Francisco, 2018.
- 739 (27) Maier, J. A.; Martinez, C.; Kasavajhala, K.; Wickstrom, L.;  
740 Hauser, K. E.; Simmerling, C. Ff14SB: Improving the Accuracy of  
741 Protein Side Chain and Backbone Parameters from Ff99SB. *J. Chem.*  
742 *Theory Comput.* **2015**, *11*, 3696–3713.
- 743 (28) Ryckaert, J. P.; Ciccotti, G.; Berendsen, H. J. C. Numerical  
744 Integration of the Cartesian Equations of Motion of a System with  
745 Constraints: Molecular Dynamics of n-Alkanes. *J. Comput. Phys.* **1977**,  
746 *23*, 327–341.
- 747 (29) Schrödinger, L. *PyMOL Molecular Graphics System*, Version 1.8;  
748 2015.
- 749 (30) Nguyen, H.; Roe, D. R.; Simmerling, C. Improved Generalized  
750 Born Solvent Model Parameters for Protein Simulations. *J. Chem.*  
751 *Theory Comput.* **2013**, *9*, 2020–2034.
- 752 (31) Compound Libraries for High Throughput/Content Screening |  
753 96-Well. [https://www.selleckchem.com/screening/fda-approved-](https://www.selleckchem.com/screening/fda-approved-drug-library.html)  
754 [drug-library.html](https://www.selleckchem.com/screening/fda-approved-drug-library.html) (accessed May 27, 2020).
- 755 (32) FDA-approved Drug Library/Targetmol96-well. [https://www.](https://www.targetmol.com/compound-library/FDA-approved-Drug-Library)  
756 [targetmol.com/compound-library/FDA-approved-Drug-Library](https://www.targetmol.com/compound-library/FDA-approved-Drug-Library) (ac-  
757 cessed May 27, 2020).
- 758 (33) Korb, O.; Möller, H. M.; Exner, T. E. NMR-Guided Molecular  
759 Docking of a Protein-Peptide Complex Based on Ant Colony  
760 Optimization. *ChemMedChem* **2010**, *5*, 1001–1006.
- 761 (34) Maffucci, I.; Contini, A. Explicit Ligand Hydration Shells  
762 Improve the Correlation between MM-PB/GBSA Binding Energies  
763 and Experimental Activities. *J. Chem. Theory Comput.* **2013**, *9*, 2706–  
764 2717.
- 765 (35) Maffucci, I.; Contini, A. Improved Computation of Protein-  
766 Protein Relative Binding Energies with the Nwat-MMGBSA Method. *J.*  
767 *Chem. Inf. Model.* **2016**, *56*, 1692–1704.
- 768 (36) Korb, O.; Stützel, T.; Exner, T. E. Empirical Scoring Functions  
769 for Advanced Protein-Ligand Docking with PLANTS. *J. Chem. Inf.*  
770 *Model.* **2009**, *49*, 84–96.
- 771 (37) Massova, I.; Kollman, P. A. Combined Molecular Mechanical  
772 and Continuum Solvent Approach (MM- PBSA/GBSA) to Predict  
773 Ligand Binding. *Perspectives in Drug Discovery and Design*; Springer,  
774 2000; pp 113–135.
- 775 (38) Choy, K.-T.; Wong, A. Y.-L.; Kaewpreedee, P.; Sia, S. F.; Chen,  
776 D.; Hui, K. P. Y.; Chu, D. K. W.; Chan, M. C. W.; Cheung, P. P.-H.;  
777 Huang, X.; Peiris, M.; Yen, H.-L. Remdesivir, Lopinavir, Emetine, and  
778 Homoharringtonine Inhibit SARS-CoV-2 Replication in Vitro.  
779 *Antiviral Res.* **2020**, *178*, 104786.
- 780 (39) Beck, B. R.; Shin, B.; Choi, Y.; Park, S.; Kang, K. Predicting  
781 Commercially Available Antiviral Drugs That May Act on the Novel  
782 Coronavirus (SARS-CoV-2) through a Drug-Target Interaction Deep  
783 Learning Model. *Comput. Struct. Biotechnol. J.* **2020**, *18*, 784–790.
- 784 (40) Hung, I. F.-N.; Lung, K.-C.; Tso, E. Y.-K.; Liu, R.; Chung, T. W.-  
785 H.; Chu, M.-Y.; Ng, Y.-Y.; Lo, J.; Chan, J.; Tam, A. R.; Shum, H.-P.;  
786 Chan, V.; Wu, A. K.-L.; Sin, K.-M.; Leung, W.-S.; Law, W.-L.; Lung, D.  
787 C.; Sin, S.; Yeung, P.; Yip, C. C.-Y.; Zhang, R. R.; Fung, A. Y.-F.; Yan, E.  
788 Y.-W.; Leung, K.-H.; Ip, J. D.; Chu, A. W.-H.; Chan, W.-M.; Ng, A. C.-  
789 K.; Lee, R.; Fung, K.; Yeung, A.; Wu, T.-C.; Chan, J. W.-M.; Yan, W.-W.;
- Chan, W.-M.; Chan, J. F.-W.; Lie, A. K.-W.; Tsang, O. T.-Y.; Cheng, V.  
C.-C.; Que, T.-L.; Lau, C.-S.; Chan, K.-H.; To, K. K.-W.; Yuen, K.-Y.  
Triple Combination of Interferon Beta-1b, Lopinavir–Ritonavir, and  
Ribavirin in the Treatment of Patients Admitted to Hospital with  
COVID-19: An Open-Label, Randomised, Phase 2 Trial. *Lancet* **2020**,  
395, 1695–1704.
- (41) Cao, B.; Wang, Y.; Wen, D.; Liu, W.; Wang, J.; Fan, G.; Ruan, L.;  
Song, B.; Cai, Y.; Wei, M.; Li, X.; Xia, J.; Chen, N.; Xiang, J.; Yu, T.; Bai,  
T.; Xie, X.; Zhang, L.; Li, C.; Yuan, Y.; Chen, H.; Li, H.; Huang, H.; Tu,  
S.; Gong, F.; Liu, Y.; Wei, Y.; Dong, C.; Zhou, F.; Gu, X.; Xu, J.; Liu, Z.;  
Zhang, Y.; Li, H.; Shang, L.; Wang, K.; Li, K.; Zhou, X.; Dong, X.; Qu,  
Z.; Lu, S.; Hu, X.; Ruan, S.; Luo, S.; Wu, J.; Peng, L.; Cheng, F.; Pan, L.;  
Zou, J.; Jia, C.; Wang, J.; Liu, X.; Wang, S.; Wu, X.; Ge, Q.; He, J.; Zhan,  
H.; Qiu, F.; Guo, L.; Huang, C.; Jaki, T.; Hayden, F. G.; Horby, P. W.;  
Zhang, D.; Wang, C. A Trial of Lopinavir-Ritonavir in Adults  
Hospitalized with Severe Covid-19. *N. Engl. J. Med.* **2020**, *382*,  
1787–1799.
- (42) Xu, L.; Liu, H.; Murray, B. P.; Callebaut, C.; Lee, M. S.; Hong, A.;  
Strickley, R. G.; Tsai, L. K.; Stray, K. M.; Wang, Y.; Rhodes, G. R.; Desai,  
M. C. Cobicistat (GS-9350): A Potent and Selective Inhibitor of  
Human CYP3A as a Novel Pharmacoenhancer. *ACS Med. Chem. Lett.*  
**2010**, *1*, 209–213.
- (43) Covid-19 clinical trials showing “encouraging” results, says  
analyst [https://www.clinicaltrialsarena.com/analysis/covid-19-](https://www.clinicaltrialsarena.com/analysis/covid-19-clinical-trials-results-2/)  
[clinical-trials-results-2/](https://www.clinicaltrialsarena.com/analysis/covid-19-clinical-trials-results-2/) (accessed Jun 1, 2020).
- (44) Lawitz, E.; Gane, E.; Pearlman, B.; Tam, E.; Ghesquiere, W.;  
Guyader, D.; Alric, L.; Bronowicki, J. P.; Lester, L.; Sievert, W.; Ghalib,  
R.; Balart, L.; Sund, F.; Lagging, M.; Dutko, F.; Shaughnessy, M.;  
Hwang, P.; Howe, A. Y. M.; Wahl, J.; Robertson, M.; Barr, E.; Haber, B.  
Efficacy and Safety of 12 Weeks versus 18 Weeks of Treatment with  
Grazoprevir (MK-5172) and Elbasvir (MK-8742) with or without  
Ribavirin for Hepatitis C Virus Genotype 1 Infection in Previously  
Untreated Patients with Cirrhosis and Patients with Previous Null  
Response with or without Cirrhosis (C-WORTHY): A Randomised,  
Open-Label Phase 2 Trial. *Lancet* **2015**, *385*, 1075–1086.
- (45) Waheed, Y. Ledipasvir and Sofosbuvir: Interferon Free Therapy  
for HCV Genotype 1 Infection. *World J. Virol.* **2015**, *4*, 33.
- (46) Zignego, A. L.; Monti, M.; Gagnani, L. Sofosbuvir/Velpatasvir  
for the Treatment of Hepatitis C Virus Infection. *Acta Biomedica.*  
Mattioli 1885 September 1, 2018; pp 321–331.
- (47) Vishal, M.; Pravin, D.; Himani, G.; Nilam, V.; Urvisha, B.; Rajesh,  
P. Drug Repurposing of Approved Drugs Elbasvir, Ledipasvir,  
Paritaprevir, Velpatasvir, Antrafenine and Ergotamine for Combating  
COVID19. Preprint. *ChemRxiv* **2020**, DOI: 10.26434/Chem-  
rxiv.12115251.V1.
- (48) Search of: ledipasvir | Covid19 - List Results - ClinicalTrials.gov  
[https://clinicaltrials.gov/ct2/results?cond=Covid19&term=](https://clinicaltrials.gov/ct2/results?cond=Covid19&term=ledipasvir&cntry=&state=&city=&dist=)  
[ledipasvir&cntry=&state=&city=&dist=](https://clinicaltrials.gov/ct2/results?cond=Covid19&term=ledipasvir&cntry=&state=&city=&dist=) (accessed Aug 27, 2020).
- (49) Waters, L.; Nelson, M. The Use of Caspofungin in HIV-Infected  
Individuals. *Expert Opin. Invest. Drugs* **2007**, *16*, 899–908.
- (50) Wang, M.; Ye, F.; Su, J.; Zhao, J.; Yuan, B.; Huang, B.; Peng, Q.;  
Peng, R.; Sun, Y.; Bai, S.; Wang, X.; Yang, W.; Fan, Z.; Wang, W.; Wu,  
G.; Gao, G. F.; Tan, W.; Sh, Y. Caspofungin and LTX-315 Inhibit  
SARS-CoV-2 Replication by Targeting the Nsp12 Polymerase. *Research*  
*Square*. Preprint. **2020**, DOI: 10.21203/RS.3.RS-19872/V1.
- (51) Yang, Y.; Cao, T.; Guo, Q. Characterization of a Traditional  
Chinese Medicine Plant the Chloroplast Genome of *Andrographis*  
*Paniculata*. *Mitochondrial DNA Part B* **2020**, *5*, 1949–1951.
- (52) Wei-Ya, C.; Yuan-Song, W.; Chun-Yu, L.; Yu-Bin, J.; Fei-Fei, Y.;  
Yong-Hong, L. Comparison of Pulmonary Availability and Anti-  
Inflammatory Effect of Dehydroandrographolide Succinate via Intra-  
tracheal and Intravenous Administration. *Eur. J. Pharm. Sci.* **2020**, *147*,  
105290.
- (53) Chen, Q.; Liu, Y.; Liu, Y. M.; Liu, G. Y.; Zhang, M. Q.; Jia, J. Y.;  
Lu, C.; Yu, C. Pharmacokinetics and Tolerance of Dehydroandrogra-  
pholide Succinate Injection after Intravenous Administration in  
Healthy Chinese Volunteers. *Acta Pharmacol. Sin.* **2012**, *33*, 1332–  
1336.

- (54) Jayakumar, T.; Hsieh, C. Y.; Lee, J. J.; Sheu, J. R. Experimental and Clinical Pharmacology of Andrographis Paniculata and Its Major Bioactive Phytoconstituent Andrographolide. *J. Evidence-Based Complementary Altern. Med.* **2013**, *2013*, 1.
- (55) Chang, R. S.; Ding, L.; Gai-Qing, C.; Qi-Choa, P.; Ze-Lin, Z.; Smith, K. M. Dehydroandrographolide Succinic Acid Monoester as an Inhibitor against the Human Immunodeficiency Virus. *Exp. Biol. Med.* **1991**, *197*, 59–66.
- (56) Cai, W.; Li, Y.; Chen, S.; Wang, M.; Zhang, A.; Zhou, H.; Chen, H.; Jin, M. 14-Deoxy-11,12-Dehydroandrographolide Exerts Anti-Influenza A Virus Activity and Inhibits Replication of H5N1 Virus by Restraining Nuclear Export of Viral Ribonucleoprotein Complexes. *Antiviral Res.* **2015**, *118*, 82–92.
- (57) Jakalian, A.; Jack, D. B.; Bayly, C. I. Fast, Efficient Generation of High-Quality Atomic Charges. AM1-BCC Model: II. Parameterization and Validation. *J. Comput. Chem.* **2002**, *23*, 1623–1641.
- (58) Bayly, C. I.; Cieplak, P.; Cornell, W. D.; Kollman, P. A. A Well-Behaved Electrostatic Potential Based Method Using Charge Restraints for Deriving Atomic Charges: The RESP Model. *J. Phys. Chem.* **1993**, *97*, 10269–10280.
- (59) Xia, S.; Liu, Q.; Wang, Q.; Sun, Z.; Su, S.; Du, L.; Ying, T.; Lu, L.; Jiang, S. Middle East Respiratory Syndrome Coronavirus (MERS-CoV) Entry Inhibitors Targeting Spike Protein. *Virus Res.* **2014**, *194*, 200–210.
- (60) Du, L.; Zhao, G.; Yang, Y.; Qiu, H.; Wang, L.; Kou, Z.; Tao, X.; Yu, H.; Sun, S.; Tseng, C.-T. K.; Jiang, S.; Li, F.; Zhou, Y. A Conformation-Dependent Neutralizing Monoclonal Antibody Specifically Targeting Receptor-Binding Domain in Middle East Respiratory Syndrome Coronavirus Spike Protein. *J. Virol.* **2014**, *88*, 7045–7053.
- (61) Li, Y.; Wan, Y.; Liu, P.; Zhao, J.; Lu, G.; Qi, J.; Wang, Q.; Lu, X.; Wu, Y.; Liu, W.; Zhang, B.; Yuen, K. Y.; Perlman, S.; Gao, G. F.; Yan, J. A Humanized Neutralizing Antibody against MERS-CoV Targeting the Receptor-Binding Domain of the Spike Protein. *Cell Res.* **2015**, *25*, 1237–1249.
- (62) Coughlin, M.; Lou, G.; Martinez, O.; Masterman, S. K.; Olsen, O. A.; Moksa, A. A.; Farzan, M.; Babcook, J. S.; Prabhakar, B. S. Generation and Characterization of Human Monoclonal Neutralizing Antibodies with Distinct Binding and Sequence Features against SARS Coronavirus Using Xenomouse®. *Virology* **2007**, *361*, 93–102.
- (63) Lei, C.; Qian, K.; Li, T.; Zhang, S.; Fu, W.; Ding, M.; Hu, S. Neutralization of SARS-CoV-2 Spike Pseudotyped Virus by Recombinant ACE2-Ig. *Nat. Commun.* **2020**, *11*, 1–5.
- (64) Zhang, G.; Pomplun, S.; Loftis, A. R.; Loas, A.; Pentelute, B. L. The First-in-Class Peptide Binder to the SARS-CoV-2 Spike Protein. *bioRxiv* **2020**, 2020.03.19.999318.
- (65) Xia, S.; Liu, M.; Wang, C.; Xu, W.; Lan, Q.; Feng, S.; Qi, F.; Bao, L.; Du, L.; Liu, S.; Qin, C.; Sun, F.; Shi, Z.; Zhu, Y.; Jiang, S.; Lu, L. Inhibition of SARS-CoV-2 (Previously 2019-nCoV) Infection by a Highly Potent Pan-Coronavirus Fusion Inhibitor Targeting Its Spike Protein That Harbors a High Capacity to Mediate Membrane Fusion. *Cell Res.* **2020**, *30*, 343–355.
- (66) Janin, J.; Chothia, C. The Structure of Protein-Protein Recognition Sites. *J. Biol. Chem.* **1990**, *265*, 16027–16030.
- (67) Spinello, A.; Saltalamacchia, A.; Magistrato, A. Is the Rigidity of SARS-CoV-2 Spike Receptor-Binding Motif the Hallmark for Its Enhanced Infectivity? An Answer from All-Atoms Simulations. *ChemRxiv*. **2020**, Preprint. DOI: 10.26434/Chemrxiv.12091260.V3.
- (68) Laha, S.; Chakraborty, J.; Das, S.; Manna, S. K.; Biswas, S.; Chatterjee, R. Characterizations of SARS-CoV-2 Mutational Profile, Spike Protein Stability and Viral Transmission. *Infect., Genet. Evol.* **2020**, *85*, 85.
- (69) Senathilake, K. S.; Samarakoon, S. R.; Tennekoon, K. H. Virtual Screening of Inhibitors against Spike Glycoprotein of SARS-CoV-2: A Drug Repurposing Approach. Preprint. **2020**, DOI: 10.20944/Preprints202003.0042.V2.
- (70) Evaluating the Use of Polymyxin B Cartridge Hemoperfusion for Patients With Septic Shock and COVID 19 <https://clinicaltrials.gov/ct2/show/NCT04352985> (accessed Jun 1, 2020).
- (71) Sajib, A. Repurposing of Approved Drugs with Potential to Block SARS-CoV-2 Surface Glycoprotein Interaction with Host Receptor. Preprint. **2020**, DOI: 10.20944/Preprints202004.0369.V1.
- (72) Belouzard, S.; Millet, J. K.; Licitra, B. N.; Whittaker, G. R. Mechanisms of Coronavirus Cell Entry Mediated by the Viral Spike Protein. *Viruses* **2012**, *4*, 1011–1033.
- (73) Liu, L.; Chopra, P.; Li, X.; Wolfert, M. A.; Tompkins, S. M.; Boons, G.-J. SARS-CoV-2 Spike Protein Binds Heparan Sulfate in a Length- and Sequence-Dependent Manner. *bioRxiv Prepr. Serv. Biol.* **2020**, 2020.05.10.087288.
- (74) Kim, S. Y.; Jin, W.; Sood, A.; Montgomery, D.; Grant, O.; Fuster, M.; Fu, L.; Dordick, J.; Woods, R.; Zhang, F.; Linhardt, R. Glycosaminoglycan Binding Motif at S1/S2 Proteolytic Cleavage Site on Spike Glycoprotein May Facilitate Novel Coronavirus (SARS-CoV-2) Host Cell Entry. *bioRxiv* **2020**, 2020.04.14.041459.
- (75) Mycroft-West Su, D.; Elli, S.; Guimond, S. E.; Miller, G. J.; Turnbull, J. E.; Yates, E. A.; Guerrini, M.; Fernig, D. G.; Lima, M. A.; de Skidmore, M. A. The 2019 Coronavirus (SARS-CoV-2) Surface Protein (Spike) S1 Receptor Binding Domain Undergoes Conformational Change upon Heparin Binding. *bioRxiv* **2020**, No. April, 2020.02.29.971093.
- (76) Nguyen, T. D.; Bottreau, E.; Aynaud, J. M. Effet Du Désoxycholate, de l'amphotéricine B et de La Fongizone Sur Le Coronavirus de La Gastroentérite Transmissible. *Ann. Inst. Pasteur/ Virol.* **1987**, *138*, 331–336.
- (77) Abobaker, A. Can Iron Chelation as an Adjunct Treatment of COVID-19 Improve the Clinical Outcome? *Eur. J. Clin. Pharmacol.* Springer, June 30, 2020; pp 1–2.
- (78) Katie, Heiser; McLean, P. F.; Davis, C. T.; Fogelson, B.; Gordon, H. B.; Jacobson, P.; Hurst, B.; Miller, B.; Alfa, R. W.; Earnshaw, B. A.; Victors, M. L.; Chong, Y. T.; Haque, I. S.; Low, A. S.; Gibson, C. C. Identification of Potential Treatments for COVID-19 through Artificial Intelligence Enabled Phenomic Analysis of Human Cells Infected with SARS-CoV-2. Preprint. *bioRxiv.* **2020**, DOI: 10.1101/2020.04.21.054387.
- (79) Chen, Y.; Li, Y.; Wang, X.; Zou, P. Montelukast, an Anti-Asthmatic Drug, Inhibits Zika Virus Infection by Disrupting Viral Integrity. *Front. Microbiol.* **2020**, *10*, 3079.
- (80) Vasanthakumar, N. Can Beta-Adrenergic Blockers Be Used in the Treatment of COVID-19? *Medical hypotheses.* NLM (Medline) May 5, 2020; p 109809.
- (81) Lamiable, A.; Thévenet, P.; Rey, J.; Vavrusa, M.; Derreumaux, P.; Tufféry, P. PEP-FOLD3: Faster de Novo Structure Prediction for Linear Peptides in Solution and in Complex. *Nucleic Acids Res.* **2016**, *44*, W449–W454.
- (82) Mascart-Lemone, F.; Huygen, K.; Clumeck, N.; Benez, D.; Bolla, K.; Duchateau, J. Stimulation of Cellular Function by Thymopentin (TP-5) in Three AIDS Patients. *The Lancet*; Elsevier, September 24, 1983; pp 735–736.
- (83) Clumeck, N.; Cran, S.; Van de Perre, P.; Mascart-Lemone, F.; Duchateau, J.; Bolla, K. Thymopentin Treatment in Aids and Pre-Aids Patients. *Surv. Immunol. Res.* **1985**, *4*, 58–62.